In Situ Characterization of Qubit Control Lines: A Qubit as a Vector Network Analyzer

Markus Jerger,[1] Anatoly Kulikov,[1,2] Zénon Vasselin,[1] and Arkady Fedorov[1,2,*]
[1]*ARC Centre of Excellence for Engineered Quantum Systems, The University of Queensland, St Lucia, Queensland 4072, Australia*
[2]*School of Mathematics and Physics, University of Queensland, Brisbane, Queensland 4072, Australia*

(Received 9 August 2017; published 9 October 2019)

We propose and experimentally realize a technique to measure the transfer function of a control line in the frequency domain using a qubit as a vector network analyzer. Our method requires coupling the line under test to the longitudinal component of the Hamiltonian of the qubit and the ability to induce Rabi oscillations through simultaneous driving of the transverse component. The method can be used to increase the fidelity of entangling gates in a quantum processor. We have demonstrated that by characterizing the "flux" control line of a superconducting transmon qubit in the range from 1 to 450 MHz and using this characterization to improve the fidelity of an entangling CPHASE gate between two transmon qubits.

DOI: 10.1103/PhysRevLett.123.150501

Signal distortions are inevitable in experiments involving radio frequency controls, where they can impact the quality of measurements and generate unwanted artifacts. In quantum control experiments and quantum information processing, these distortions are the source of errors and may limit the fidelity of operations. Quantum gates that use nonadiabatic (fast) frequency tuning of the qubits involved are particularly sensitive to distortion and require precise calibration [1–6]. Distortion can be canceled, in principle, if the complex transfer function of the control line is known, by applying its inverse to the signal before it is transmitted. The most common approach to obtain the transfer function is to measure it [at room temperature (RT)] in the frequency domain using a vector network analyzer or in the time domain using an oscilloscope (see, e.g., Ref. [5]).

This method has two important deficiencies: the transfer function of the line changes when the setup is cooled to cryogenic temperatures, and the part of the signal line from the microwave connector closest to the chip to the qubit is not included in the characterization. Various methods for *in situ* line calibration have been proposed. Some calibration methods are limited in time resolution by the length of the microwave π pulse [1,3,5], others are applicable only to specific systems [2] or pulses [7], and most procedures only provide indirect information about the transfer function.

In this Letter we propose and experimentally realize a method of *in situ* direct reconstruction of the response of a control line of a qubit using the qubit itself. The accuracy of our method is limited by decoherence of the qubit at low frequencies. At high frequencies the accuracy is fundamentally limited by the rotating wave approximation (see Supplemental Material [8]). We benchmark the method by measuring the transfer function of an element introduced at room temperature and comparing the measured response with the response obtained by using a commercial vector network analyzer (VNA). We then apply the method to improve the fidelity of a nonadiabatic controlled phase (CPHASE) gate [12,13] between two transmon qubits, one of the most commonly used entangling gates in superconducting systems.

To understand the principles underlying our method, consider the Hamiltonian of a qubit with time-dependent longitudinal (frequency control) and transverse (excitation) drives:

$$H = \frac{\hbar}{2}\omega_0\sigma_z + \hbar A_x \cos(\omega_x t + \phi_x)\sigma_x + \hbar A_z \cos(\omega_z t + \phi_z)\sigma_z. \quad (1)$$

After transformation into the rotating frame with $U_1 = e^{i(\omega_x t+\phi_x)\sigma_z/2}$, the Hamiltonian reads

$$H' = \frac{\hbar}{2}A_x\sigma_x' + \frac{\hbar}{2}\delta\omega\sigma_z' + \hbar A_z \cos(\omega_z t + \phi_z)\sigma_z', \quad (2)$$

where $\delta\omega = \omega_0 - \omega_x$ is the detuning of the excitation driving and we have used the rotating wave approximation under the assumption $A_x \ll \omega_0$. Note that the transverse phase ϕ_x does not explicitly appear in the Hamiltonian (2); however, it implicitly provides a reference for the rotating frame through the transformation operator U_1. The time-independent part of H' can be diagonalized with $U_2 = e^{i\phi_t\sigma_y'/2}$, $\phi_t = \arctan(\delta\omega/A_x)$, as

$$\tilde{H}' = \frac{\hbar}{2}\Omega_R\tilde{\sigma}_x' + \hbar\omega_R \cos(\omega_z t + \phi_z)\tilde{\sigma}_z' + \hbar\omega_R\frac{\delta\omega}{A_x}\cos(\omega_z t + \phi_z)\tilde{\sigma}_x', \quad (3)$$

where $\Omega_R = \sqrt{A_x^2 + \delta\omega^2}$ is the Rabi frequency and $\omega_R = A_z A_x/\Omega_R$. In the special case of $\delta\omega = 0$, U_2 reduces to the identity, $\Omega_R = A_x$ and $\omega_R = A_z$.

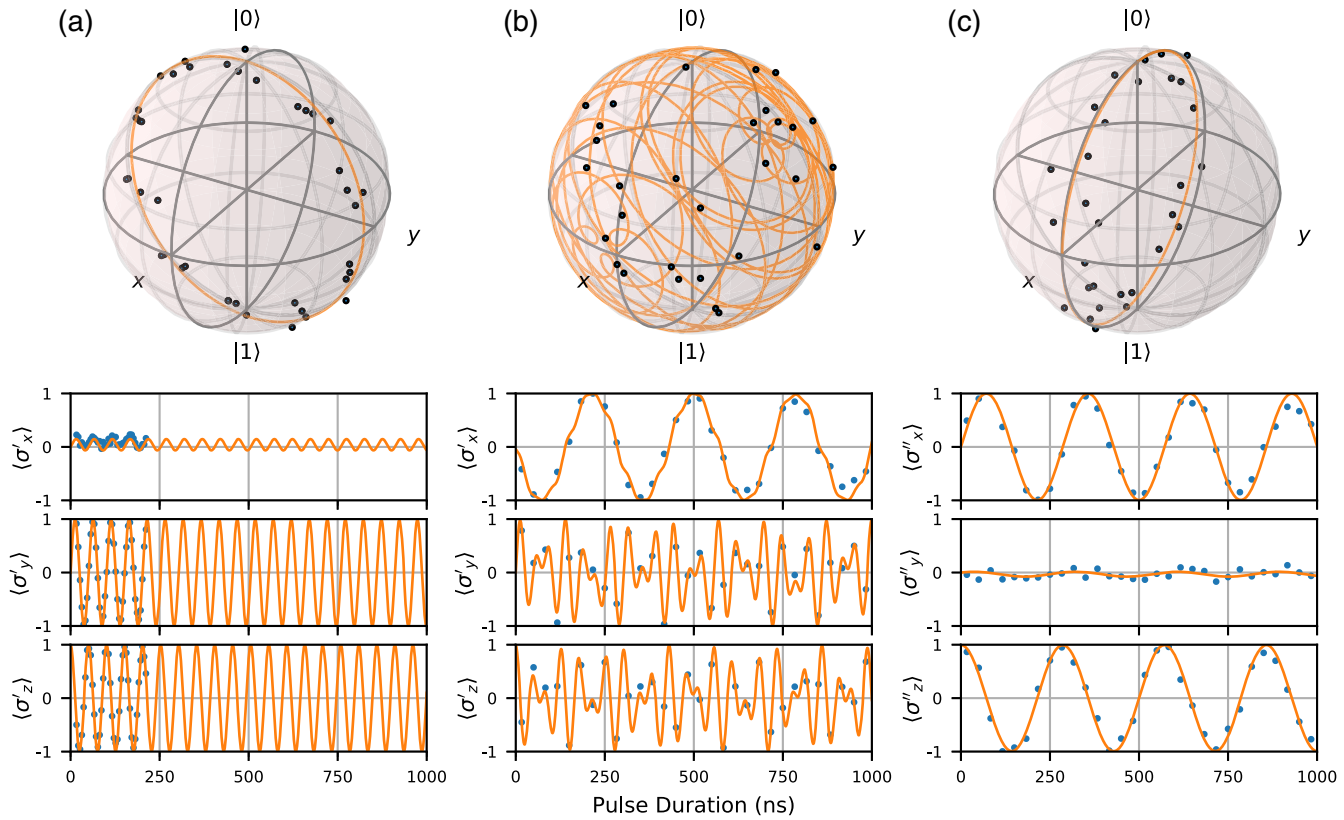

FIG. 1. A typical dataset for $\Omega_R = 19.8$ MHz and the corresponding trajectories of the Bloch vector in the first rotating frame with only the x drive applied, with x and z drives and with x and z drives in the second rotating frame. (a) State tomography of the qubit with only the x drive applied. The fit yields a rotation vector of $\vec{\Theta} = (19.7, -1.9, 0.8)$ MHz and $\phi_x = -0.1$. (b) State tomography of the qubit with both the x and z drives applied. The frequency of z drive is set to $\omega_z = \Omega_R$. The sampling rate of the experiment is chosen such that the slow oscillations at ω_R can be resolved unambiguously but not necessarily the fast oscillations at Ω_R, which are canceled by U_3. The orange curve shows the theoretical dynamics derived from the fit in (c). (c) The dynamics of the qubit in the second rotating frame, transformed from (b). The fit yields $\vec{\theta} = (0.2, -3.5, 0.1)$ MHz, and we can obtain $A_z = 3.51$ MHz and $\phi_z = -1.54$.

Comparing Eqs. (1) and (3), we observe that in the rotating frame the z term plays the role of a transverse drive for the dressed-state qubit with splitting Ω_R and will induce Rabi oscillations of the dressed-state qubit with frequency ω_R. To make this observation explicit we transform the Hamiltonian (3) into the second rotating frame for $\omega_z = \Omega_R$, with $U_3 = e^{i(\omega_z t)\tilde{\sigma}'_x/2}$, to obtain

$$H'' = \frac{\hbar}{2}\omega_R(\sin\phi_z\sigma''_y + \cos\phi_z\sigma''_z), \tag{4}$$

where we have used another rotating wave approximation with $\omega_R \ll \Omega_R$. The Hamiltonian H'' shows that the amplitude A_z and phase ϕ_z of the z control are encoded in the frequency and axis of the Rabi oscillations of the dressed-state qubit and can be measured in the experiment.

The experimental procedure is summarized by the following steps.

(i) Apply x drive with z drive off ($A_z = 0$) and fit data to extract Ω_R [Fig. 1(a)].

(ii) Set $\omega_z = \Omega_R$, apply both x and z drives, and use tomography pulses to reconstruct $\langle\sigma'_x(t)\rangle$, $\langle\sigma'_y(t)\rangle$, and $\langle\sigma'_z(t)\rangle$ in the first rotating frame [Fig. 1(b)].

(iii) Postprocess the data to reconstruct $\langle\sigma''_x(t)\rangle$, $\langle\sigma''_y(t)\rangle$, and $\langle\sigma''_z(t)\rangle$ in the second rotating frame. Fit the resulting data to Rabi oscillations described by Eq. (4) to extract A_z and ϕ_z for given ω_z [Fig. 1(c)].

(iv) Repeat the sequence for different Ω_R to cover the necessary frequency range.

Both A_z and phase ϕ_z for a given frequency ω_z can be determined directly from the observables in the laboratory or the first rotating frames, such as the excited state population of the qubit (for the sensitivity of the method to ϕ_z, see Supplemental Material [8]). However, it is more convenient to perform tomography and reconstruct the oscillation of the qubit state in the second rotating frame by postprocessing. Removing the fast population oscillation with frequency Ω_R and leaving only the signal varying with the frequency ω_R allows for a substantial reduction of the required sampling rate and more robust fitting.

By setting $\delta\omega = 0$ and varying A_x one can perform the experiment for different ω_z and identify the transfer function of the z line in the range of frequencies Γ_1, $\Gamma_2 \ll \omega_z \ll \omega_0$, which are most relevant for the frequency

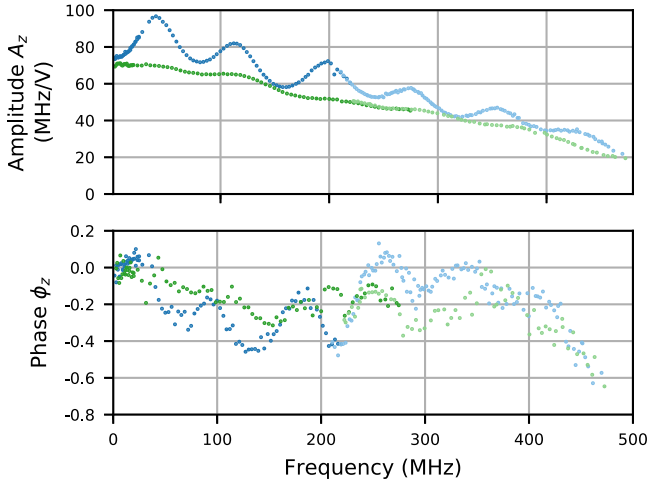

FIG. 2. Amplitudes A_z and phases ϕ_z of the transfer functions of the z control line. Points in blue and green show the response of the flux line for two different configurations (see text for details). Darker points were measured with resonant driving $\omega_x = \omega_0$ by varying A_x, lighter points were measured by varying $\omega_x - \omega_0$ with fixed A_x (off-resonant case).

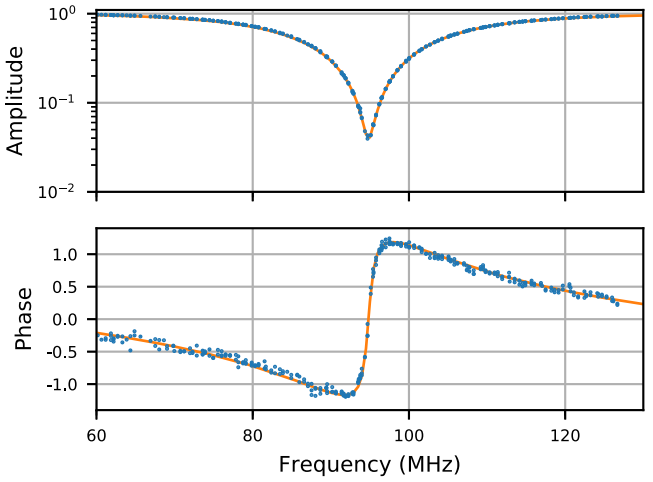

FIG. 3. Amplitude and phase of transmission through a transmission line with a shorted stub resonator. Points in blue were measured with the qubit by comparing A_z and ϕ_z with and without the stub in place, the orange line was measured directly with a commercial vector network analyzer.

control of the qubit with $\Gamma_{1,2}$ being the relaxation and dephasing rates of the qubit, respectively. The idea of scanning the Rabi frequency was also used to perform noise spectroscopy [14,15] utilizing the dependence of the Rabi decay time on the Rabi frequency [16]. For highly anharmonic flux qubits, Rabi frequencies of up to 1.7 GHz were achieved [15].

For weakly anharmonic qubits, such as the transmon, the two-level approximation breaks down when A_x starts being a considerable fraction of the anharmonicity, about 350 MHz for the qubits used here. To mitigate this problem, we can exploit off-resonant driving ($\delta\omega < 0$), which increases the Ω_R at the same A_x and also allows higher A_x because the frequency of the drive is farther from the frequency of the $|1\rangle$-$|2\rangle$ transition. This allows us to extend the analysis to higher frequencies at the expense of signal amplitude.

We describe the experimental steps in more detail and directions for efficient implementation of the procedure in Supplemental Material [8]. We have tested our method on a standard circuit quantum electrodynamics system: a transmon qubit coupled to a readout resonator with local charge and flux lines. More specifically, we choose QB2 of a chip virtually identical to one used in Ref. [17].

With our method we characterized the complex transfer function in the range of 1–450 MHz (Fig. 2). Each point was taken with 4096 averages at a repetition rate of 40 kHz. The measurements at lower frequencies were limited by decoherence of the qubit. However, we point out that the low frequency part of the transfer function can also be measured with other methods with lower time resolution [1,3].

At high frequencies our accuracy is limited by population of the higher levels for the resonant driving case and by the loss of signal contrast at large detunings in the off-resonant driving case. In addition, the amplitude reconstruction is more robust as it corresponds to the frequency of the oscillations while the phase is reconstructed from a ratio of their amplitudes.

We have benchmarked our method by introducing an additional element in the flux line at room temperature. We used a shorted stub resonator made from a BNC T adapter and several meters of a BNC cable shorted at the end. We repeated the characterization of the line with the element and used the original data for the line to de-embed the transfer function of the element itself. The result is shown in Fig. 3 in comparison with the transfer function of the element measured separately with the commercial vector network analyzer. The agreement between our method and the VNA is excellent, showing the dynamic range of our method for measuring amplitude of $\simeq$30 dB. The dynamic range of a single measurement is bounded by the condition $\omega_R \ll \Omega_R$ required for the rotating wave approximation in Eq. (4) and the decoherence time of the qubit. It can be further improved by dynamically changing the amplitude of the z drive, taking advantage of the dynamic range of the arbitrary waveform generator (AWG).

We have employed the outlined method of flux line calibration to improve the quality of a CPHASE entangling gate between two superconducting transmon qubits. The gate between two transmons can be realized [12,13] by bringing the second excited state $|02\rangle$ of one qubit in resonance with the $|11\rangle$ state where both qubits are excited, inducing energy exchange between the states. On each swap of an excitation the state acquires a phase of $\pi/2$, so that a system starting in $|11\rangle$ evolves into $i|02\rangle$ and subsequently into $-|11\rangle$. Since one of the qubits must be tuned in frequency, there is an additional dynamical phase acquired by the qubit which must

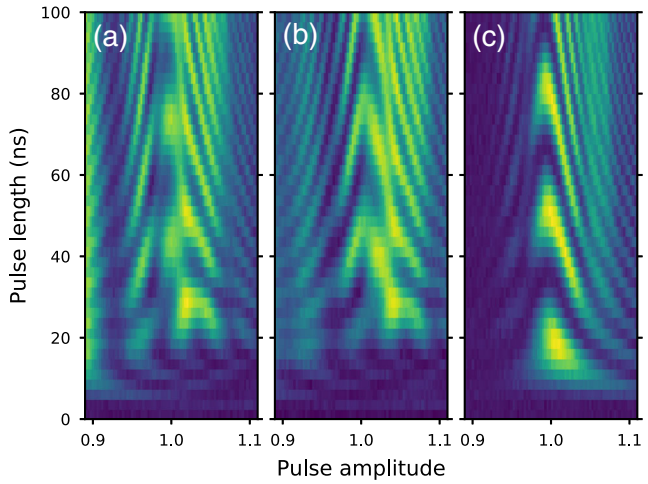

FIG. 4. Vaccum Rabi oscillation between the $|11\rangle$ and $|20\rangle$ states of two transmon qubits assuming (a) a perfect impulse response, (b) the impulse response measured at room temperature, and (c) the impulse response measured using the qubit.

be accounted for. Apart from that, the other computational basis states, $|00\rangle$, $|10\rangle$, and $|01\rangle$ are unaffected by the gate.

To implement the gate we used QB1 and QB2 of the chip, both parked at their symmetry points at frequencies 5.5 and 6.5 GHz, respectively. We tune QB2 near ~5.8 GHz to allow the states $|11\rangle$ and $|02\rangle$ to exchange excitation via virtual photons in a common transmission line resonator.

An ideal CPHASE gate requires a perfect step pulse, which cannot be implemented by any physical device. In order to comply with the bandwidth limitation of our AWG and to make the distortion correction easier, we applied a Gaussian low-pass filter with a cutoff frequency of 300 MHz to the ideal square pulse shape. This pulse shape was programmed to the AWG and was used to implement the CPHASE gate.

To calibrate the amplitude and duration of the flux pulse, we prepared qubits in $|11\rangle$ followed by the flux pulse on QB2 where we sweep both the length and the amplitude of the pulse. Measurement of the resonator response shows characteristic oscillations (often called "chevron patterns") manifesting excitation exchange between $|11\rangle$ and $|02\rangle$ states of the two transmons. The pattern is distorted due to extra reflections on the flux line which appear only at low temperatures and cannot be calibrated at room temperatures [the reflections of the line can be seen as broad resonances in the line frequency response; see Fig. 4(a)].

Following the most common approach to compensate for these distortions, we have measured the room temperature impulse response of the flux line before cooling down the refrigerator. We then used the standard machinery [5] to compute the necessary waveform which then can be loaded to AWG to yield the desired pulse shape. Using this computed pulse shape, we repeated the calibration routine [Fig. 4(b)], but the oscillations remain heavily distorted. In particular, one may note that the oscillations start only after the first 15 ns, which we attribute to a large overshoot in the actual flux pulse.

With our *in situ* calibration of the flux line (the response in blue in Fig. 2) for distortion compensation, we have measured the improved oscillation pattern shown in Fig. 4(c). The oscillations' visibility is asymmetric, which we attribute mostly to the bandwidth limitations of the pulse shape. Apart from that the compensation fixes most of the imperfections and, more specifically, the oscillations begin without delay at short lengths of the flux pulse.

To quantify our method, we have calibrated the CPHASE gate with no correction, with RT correction, and our *in situ* correction. Applying our method, the process fidelity of the gate increases from 0.835 ± 0.015 to 0.875 ± 0.01. Numerical simulation of the protocol with the experimental values of $T_1 = 2.5\ \mu$s and $T_2 = 1.4\ \mu$s and perfect pulse shape showed the process fidelity of 0.885. Contrary to our initial expectations, applying the RT calibration has not improved the fidelity of the gate.

During a later cooldown we introduced extra attenuation to the resonator input and flux lines which increased the coherence of the qubits to $T_1 = 4\ \mu$s, $T_2 = 4.5\ \mu$s and reassembled the flux control line. In this configuration we were unable to demonstrate a statistically significant improvement in the fidelity of the CPHASE gate, neither with RT calibration nor with *in situ* calibration. The process fidelity was measured to be 0.945, which was predominately limited by decoherence of the transmons. *In situ* measurement of the frequency response of the line (Fig. 2, green curves, rescaled for the extra attenuation) did not show the characteristic resonances seen previously (Fig. 2, blue curves). Both measurements reinforce our statement that using the qubit as a VNA allows one to precisely characterize the qubit control lines in a methodical manner and improve the fidelity of entangling gates if the control signals' distortions contribute significantly to the infidelity.

Our method is the first direct *in situ* measurement of the line transfer function from room temperature electronics to a qubit on a chip. The method is most relevant for superconducting qubits whose frequencies are routinely tuned but is applicable for all qubits with z and x control. For superconducting qubits one can use our procedure to improve the fidelity of the two-qubit quantum gates [12,13,18,19] as well as photon-qubit operations requiring nonadiabatic control [1,4,6]. In addition to quantum control applications, the qubit can also be used as a microscopic probe of the electromagnetic fields in frequency domain.

We thank Steffen Schlör for his help with the experiment. M. J., A. K., and A. F. were supported by the Australian Research Council Centre of Excellence CE170100009. A. F. was supported by the ARC Future Fellowship FT140100338.

M. J. and A. K. contributed equally to this work.

Note added.—Recently, we became aware of a complementary time-domain method [20] employing a qubit as an oscilloscope, which allows one to sample control pulses of arbitrary shape making use of nonlinear qubit frequency dependence on flux.

*a.fedorov@uq.edu.au

[1] M. Hofheinz, H. Wang, M. Ansmann, R. C. Bialczak, E. Lucero, M. Neeley, A. D. O'Connell, D. Sank, J. Wenner, J. M. Martinis, and A. N. Cleland, Nature (London) **459**, 546 (2009).

[2] J. Bylander, M. S. Rudner, A. V. Shytov, S. O. Valenzuela, D. M. Berns, K. K. Berggren, L. S. Levitov, and W. D. Oliver, Phys. Rev. B **80**, 220506(R) (2009).

[3] B. Johnson, Controlling photons in superconducting electrical circuits, Ph.D. thesis, Yale University, 2011.

[4] D. Bozyigit, C. Lang, L. Steffen, J. M. Fink, C. Eichler, M. Baur, R. Bianchetti, P. J. Leek, S. Filipp, M. P. da Silva, A. Blais, and A. Wallraff, Nat. Phys. **7**, 154 (2011).

[5] M. Baur, Realizing quantum gates, and algorithms with three superconducting qubits, Ph.D. thesis, ETH Zurich, 2012.

[6] N. K. Langford, R. Sagastizabal, M. Kounalakis, C. Dickel, A. Bruno, F. Luthi, D. J. Thoen, A. Endo, and L. DiCarlo, Nat. Commun. **8**, 1715 (2017).

[7] S. Gustavsson, O. Zwier, J. Bylander, F. Yan, F. Yoshihara, Y. Nakamura, T. P. Orlando, and W. D. Oliver, Phys. Rev. Lett. **110**, 040502 (2013).

[8] See Supplemental Material at http://link.aps.org/supplemental/10.1103/PhysRevLett.123.150501 for a detailed description of the experimental procedure, error analysis, and sensitivity of the method, which includes Refs. [9–11].

[9] F. Bloch and A. Siegert, Phys. Rev. **57**, 522 (1940).

[10] D. Zeuch, F. Hassler, J. Slim, and D. DiVincenzo, arXiv:1807.02858.

[11] J. R. Johansson, P. D. Nation, and F. Nori, Comput. Phys. Commun. **184**, 1234 (2013).

[12] F. W. Strauch, P. R. Johnson, A. J. Dragt, C. J. Lobb, J. R. Anderson, and F. C. Wellstood, Phys. Rev. Lett. **91**, 167005 (2003).

[13] L. DiCarlo, J. M. Chow, J. M. Gambetta, L. S. Bishop, B. R. Johnson, D. I. Schuster, J. Majer, A. Blais, L. Frunzio, S. M. Girvin, and R. J. Schoelkopf, Nature (London) **460**, 240 (2009).

[14] J. Bylander, S. Gustavsson, F. Yan, F. Yoshihara, K. Harrabi, G. Fitch, D. G. Cory, Y. Nakamura, J.-S. Tsai, and W. D. Oliver, Nat. Phys. **7**, 565 (2011).

[15] F. Yoshihara, Y. Nakamura, F. Yan, S. Gustavsson, J. Bylander, W. D. Oliver, and J.-S. Tsai, Phys. Rev. B **89**, 020503(R) (2014).

[16] G. Ithier, E. Collin, P. Joyez, P. J. Meeson, D. Vion, D. Esteve, F. Chiarello, A. Shnirman, Y. Makhlin, J. Schriefl, and G. Schön, Phys. Rev. B **72**, 134519 (2005).

[17] L. Steffen, Y. Salathe, M. Oppliger, P. Kurpiers, M. Baur, C. Lang, C. Eichler, G. Puebla-Hellmann, A. Fedorov, and A. Wallraff, Nature (London) **500**, 319 (2013).

[18] R. C. Bialczak, M. Ansmann, M. Hofheinz, E. Lucero, M. Neeley, A. D. O'Connell, D. Sank, H. Wang, J. Wenner, M. Steffen, A. N. Cleland, and J. M. Martinis, Nat. Phys. **6**, 409 (2010).

[19] T. Yamamoto, M. Neeley, E. Lucero, R. C. Bialczak, J. Kelly, M. Lenander, M. Mariantoni, A. D. O'Connell, D. Sank, H. Wang, M. Weides, J. Wenner, Y. Yin, A. N. Cleland, and J. M. Martinis, Phys. Rev. B **82**, 184515 (2010).

[20] M. A. Rol, L. Ciorciaro, F. K. Malinowski, B. M. Tarasinski, R. E. Sagastizabal, C. C. Bultink, Y. Salathe, N. Haandbaek, J. Sedivy, and L. DiCarlo, arXiv:1907.04818.